Microsyst Technol (2009) 15:1233–1243
DOI 10.1007/s00542-009-0820-7

TECHNICAL PAPER

Design methodology and fabrication process of a microinductor for the next generation of DC–DC power converters

David Flynn · Marc P. Y. Desmulliez

Received: 17 June 2008 / Accepted: 13 March 2009 / Published online: 7 April 2009

Abstract Magnetic materials used in cored microinductors to supersede ferrite in the 0.5-10 MHz frequency range are investigated in this article. The performance of electrodeposited nickel–iron, cobalt–iron–copper alloys and the commercial alloy Vitrovac 6025 have been assessed through their inclusion within a custom-made solenoid microinductor. Although the present inductor achieves 77% power efficiency at 500 KHz for 24.7 W/cm^3 power density, an optimized process predicts a power efficiency of 97% for 30.83 W/cm^3 power density. The main issues regarding microinductor design and performance are discussed.

1 Introduction

There is an increasing demand for miniaturised power inductors and transformers that can be operated at high frequency either on a chip or on a module (Huljak et al. 2000; Lotfi et al. 2001; ITRS 2001). These inductive components have used either to power hand-held mobile electronic systems, locally distributed Points of Load (PoL) or power conversion electronic systems. The trend towards the miniaturisation of these components has resulted in the development of surface-mount devices that are lower in profile than traditional bulk components. However, since these surface mount devices are inherently developed from existing conventional bulk technology, the ability to produce further improvements is limited in terms of component profile, increased power density or level of integration. There is a demand therefore for a fabrication technology based on MEMS manufacturing processes for high power density, low profile, and highly efficient passive inductive components.

1.1 Motivation for microscale magnetic component

While the physical size of digital and analogue electronic circuits has been drastically reduced over the past 20 years, their associated power supplies have shrunk at a much slower rate. As a result, the power supply represents an increasing proportion of the size and cost of electronic equipment. One of the main difficulties in the miniaturization of power conversion circuits such as DC–DC converters is the manufacturing of small inductors and transformers. As expressed as far back as 1988, "magnetic design is the main bottleneck to the successful reduction of the overall converter size and weight" (Goldberg 1988).

Recent efforts to miniaturise the overall size of DC–DC power converters has resulted in an increase in switching frequency of the power circuit from the 100–500 kHz range to the 1–10 MHz range. This effort has led to a reduction of the size of the energy storage components that dominate the converter volume, as shown in Fig. 1a and b (Lotfi et al. 2001). Several problems arise with power circuits operating into the MHz frequency region. Core materials such as MnZn ferrites, which are commonly used in the 20–500 kHz region, have rapidly increasing hysteresis and eddy current losses as the frequency is increased. Eddy current losses in windings can also become a severe problem, as the skin depth in copper becomes small compared to the cross section of the windings.

D. Flynn (✉) · M. P. Y. Desmulliez
MIcroSystems Engineering Centre (MISEC),
School of Engineering and Physical Sciences,
Heriot-Watt University, Earl Mountbatten Building,
Edinburgh EH14 4AS, UK
e-mail: d.flynn@hw.ac.uk

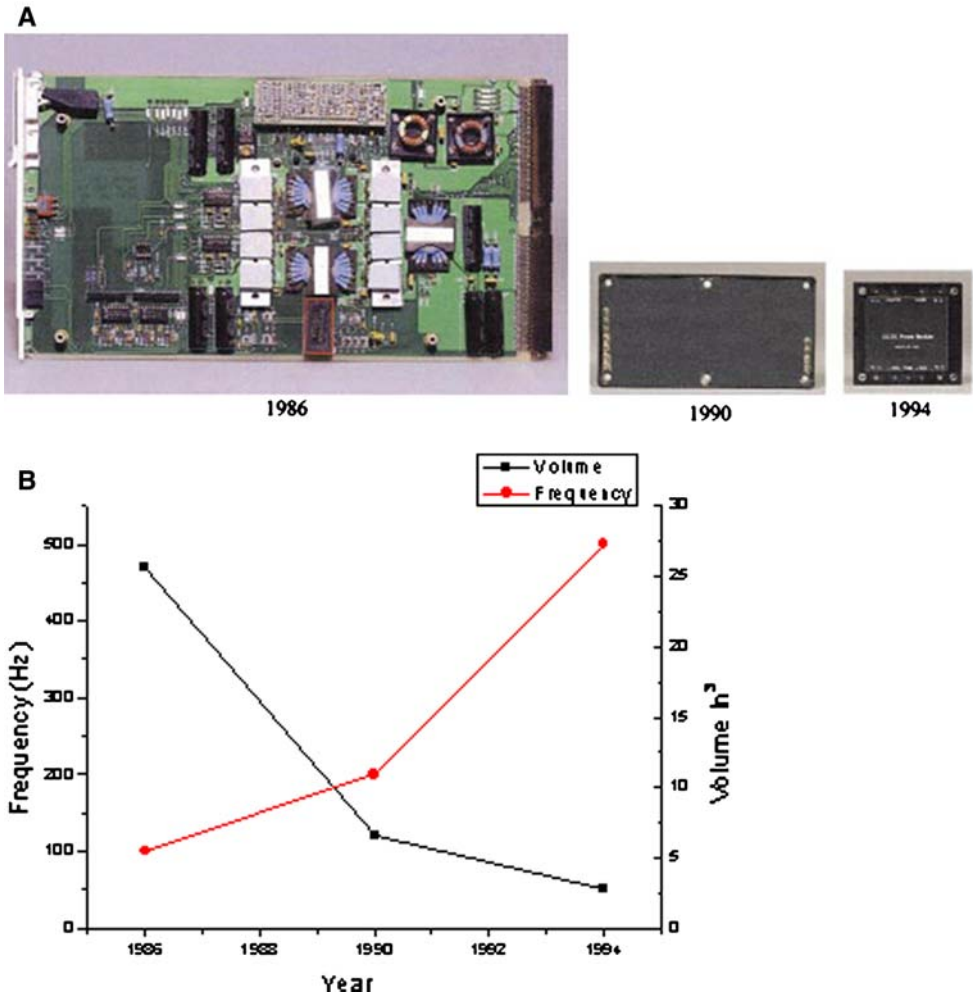

Fig. 1 **a** Evolution of the size of telecommunication power modules. The modules shown operate at the same power and voltage levels. Large energy storage elements required at lower frequencies have given way to smaller elements at higher frequencies. **b** The increase in operating frequency has reduced the size of the bulky passive components

In the magnetic recording head industry, thin-film metal alloys have replaced ferrites as the material of choice for inductive read-write heads, particularly where high density and high frequency are required. These materials have high saturation flux density and the use of thin films controls eddy current losses at frequencies up and above 100 MHz (Jagielinski 1990; Kohmoto 1991). Structures with very small feature size are fabricated used photolithography techniques borrowed from the microelectronics industry.

The materials and fabrication techniques used for magnetic recording heads show much promise for high frequency power conversion. The ability to fabricate very fine patterning can reduce eddy current losses in both cores and windings. The higher saturation flux density of the magnetic alloys, as compared to that of ferrites, allows high power density in small planar devices. While costs may initially be high, batch processing techniques can bring the cost down substantially, and mass-produced devices may be significantly less expensive than conventional wound magnetic circuit elements. The cost breakdown is in fact different from that of conventional magnetic devices as it is related to the number of layers and substrate area, rather than the number of turns.

1.2 Market trends of passive power components

All electronic devices have a power supply. The market place, until recently, did not stimulate however the necessary technological development for improved power supply in terms of power density and efficiency since customers were unwilling to pay more for enhanced power supply. This behaviour is to be contrasted with the strong investment made in high performance processors as a result of market demand (ITRS 2001). Hence the economic incentive to push for dramatically higher power-supply densities was not there.

Today's consumer products are the main driver of the electronics industry. The increasing functionality of electronic products and demands for increased operation time have produced a surge in power density requirement. More and more, portable electronic products prioritise power over performance due to their reliance on battery operation.

Small DC–DC converters may be the key enablers in powering high performance loads, and there is now a growing economic incentive to invest in the needed technology improvements. Frost and Sullivan (F & S) predict that the entire power supply industry will grow at a compound annual growth rate (CAGR) of 6.5% through 2009, bringing revenues of $15.6 billion. By 2009 the revenue share of the DC–DC modules within this market will grow to 41.7% from 35.6% in 2002 (Wong et al. 2004).

Addressing consumer needs will require price competitive components but initial markets for miniaturised converters are in equipment whose size and weight must be minimised, such as in aerospace and avionics applications. These products are produced in low volume and their performance and reliability take precedence over cost, especially for military applications.

1.3 Technology drivers of passive power components

A number of scientific studies have addressed the issue of the technological changes that need to take place to for the power supply of the future. The findings of the Power Sources Manufacturers Association (PSMA) are presented in Fig. 2 (PSMA 2000). Solutions lie in the categories of packaging, circuits and technology, passive components and semiconductors.

As shown in Fig. 2, cost are to be reduced through optimal topologies, more integration, innovative design and manufacturing techniques. Time-to-market will be shortened through integration and design software. Power density will increase with higher frequency, more integration, lower losses, better components and thermal design. The growth in switching frequency will be via better components, lower losses, thermal design and the development of new materials. Reliability will be improved with better design, better components and thermal design. As a result, reduced power loss will be achieved with optimal topologies, better components and power semiconductors.

Another study, the International Technology Roadmap for Semiconductors (ITRS Roadmap), confirms the trend outlined by the PSMA as far as the hand-held electronic product sector is concerned (ITRS 2001). Based on this roadmap, the graph in Fig. 3 plots the estimated trends in output power, voltage and current for a single buck DC–DC converter supplying power to the digital section of a handheld electronic product. The general trend is an increase in power consumption of up to 3 W, with a decrease in voltages (down to 0.8 V in 2010) resulting in an increase of output current from 2 to 5 A. For illustration purposes, given the estimates for DC–DC converter power, current and voltage, it is relatively easy to determine, for a given switching frequency, the inductance and capacitance values required to satisfy any given specifications for current and voltage ripple. If the switching frequency of the converter remains constant at 1 MHz the capacitance requirements will increase by a factor of 2.25 by 2010 while the inductance will be reduced by a factor of 2.

Clearly, to achieve miniaturization, a decrease in both capacitor and inductor values addresses this increase in converter switching frequency. The next limitation in going

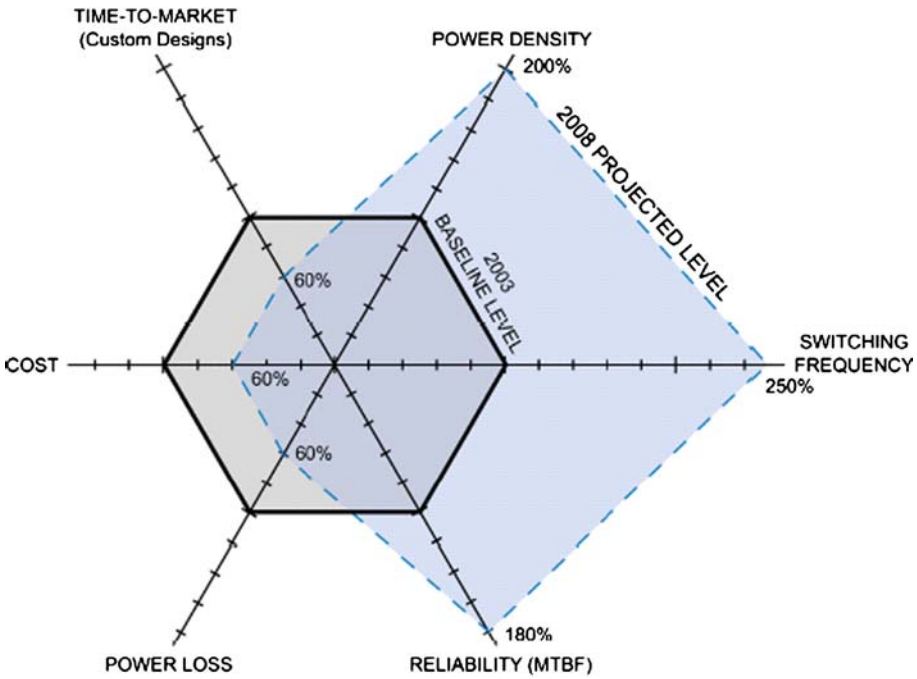

Fig. 2 "A 5-year power technology roadmap'' [PSMA 2000]

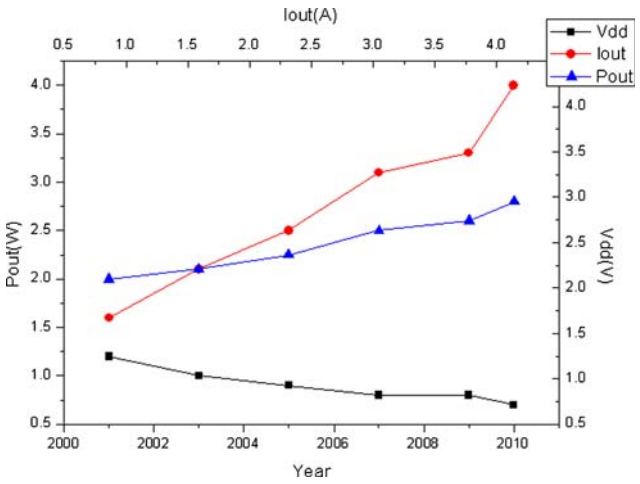

Fig. 3 Estimation of the output power, voltage and current for a single buck converter supply in handheld electronic products

to higher switching frequencies is the magnetic components within the circuit. Since switching frequency stalled in the few hundred kHz range (Huljak et al. 2000, ITRS 2001), magnetic core manufacturers focused their development efforts on developing core materials with reduced loss in this frequency range. Ferrites appear to have reached maturity in terms of higher frequency operation at reasonable loss levels. Therefore new core materials applicable at frequencies of 10 MHz and beyond need to be developed. Another concern in the area of magnetic components is the windings. With increasing frequency the magnetic component becomes smaller, AC resistance losses increase alongside the current handling capability of the windings.

2 Inductor design

2.1 Magnetic core geometry

For optimal component configuration, a comparison has to be made across a variety of factors which include power handling capability, output power efficiency, practicality of fabrication, inductance requirement, etc. Consider a core material for a one-turn micro-inductor. The saturation flux density, B_{sat} ,

$$B_{\text{sat}} = \frac{\mu_{\text{o}}\mu_{\text{r}}NI}{l_{\text{c}}} \tag{1}$$

is a predetermined constant as it is a property of the magnetic material that forms the core of the inductor. In the same way, the current applied to the component is known for a given application. Therefore, the only free parameter left will be either the relative permeability or the flux path length, since

$$\frac{l_{\text{c}}}{\mu_{\text{r}}} = \frac{I\mu_{\text{o}}}{B} \tag{2}$$

The magnetic core, whose cross-section is typically a rectangle, triangle or a circle, has a certain perimeter. Consider a rectangular core within a one turn pot-core component, as shown in Fig. 4. In this figure the main flux path is indicated. With increased frequency, the skin depths of the magnetic material and windings decrease. Therefore, to minimise skin depth losses and maintain the inductance value, the device must become thinner and wider. The resulting increase in the length of the flux path requires a higher value of the relative permeability for the inductance value to stay constant. An increase in relative permeability for the same resistivity value will make the material susceptible to skin depth losses at reduced frequency.

If, for the same area and core material, the rectangular geometry was changed to a triangular geometry, then the perimeter is reduced by one-third. The required permeability is then reduced by 1/3 and greater skin depth is achieved for the same resistivity. A one turn micro-inductor with a triangular trench structure was fabricated by Sullivan et al. (Sullivan et al. 2003). The fabrication of this V-groove micro-inductor required sputter deposition. Sputtering is a slow and costly process, and due to delamination can only be used for small core areas. Sect. 4 will demonstrate how limiting the number of laminate layers in a magnetic core can have an adverse effect on component performance.

A circular component would suffer from the same technical disadvantages as the triangular component. Moreover, a circular component fabricated by micromachining methods would require non-planar construction. Minimal footprint and low profile are prerequisites for present and future magnetic components. Therefore, a circular component was not investigated. Due to the aforementioned complications of triangular and circular geometries, the investigated components herein are of rectangular planar form. Disadvantages of this geometry will be overcome by tailoring the core properties and the design of the component.

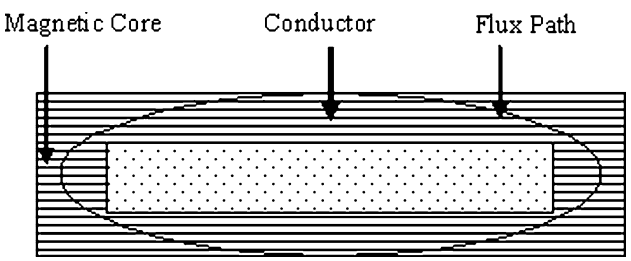

Fig. 4 A simple rectangular one-turn micro-inductor

2.2 Winding geometry

The winding geometries generally encountered for the inductor are of the spiral, meander or solenoid forms. A single layer solenoid component allows near ideal performance (Flynn et al. 2007). The number of turns per single layer of traditionally wound solenoid inductors is limited by the inner diameter of the core and how tightly the turns can be packed together. To increase inductance, a larger core or multiple layers of windings would normally be needed. This would normally lead to an increase in component size and parasitic capacitance. UV-photolithography used for the manufacturing of the solenoid allows a higher winding density.

An important issue in choosing a winding configuration is the magnitude and distribution of external magnetic fields generated by the transformer or inductor. The conventional pot-core is better at minimizing external magnetic fields, as the core encloses and, in so doing, shields the windings. This shielding results in low external fields regardless of the distribution of primary and secondary windings inside the core. Solenoid components also have low external fields due to the winding distribution. In transformer applications the primary and secondary windings are customarily distributed evenly around the core and lie on top of each other with little space in between. The currents cancel each other, so little external field results. In micro-fabrication the ability to pattern fine windings makes it relatively easy to arrange the windings so that primary and secondary currents locally cancel. Hence, external fields are not a primary concern in component development.

Perhaps the most important factor in comparing the pot-core, spiral and solenoid designs is the ease of manufacture. This parameter is the most difficult to quantify and obviously dependent on fabrication capability. In the solenoid case, a difficulty often encountered is the interconnection of the top and bottom winding layers to encircle the core. This requires accurate alignment between the layers to insure proper connections, low-resistance contacts and connection over a vertical distance greater than the thickness of the core. A customed flip-chip bonding procedure overcomes the aforementioned difficulties (Flynn et al. 2007).

In the pot core design, the inter-layer connection requirements are less severe because the windings are planar and manufactured in a single deposition process. A complication arises if the inductor winding is spiral as access to the output pad is required. This typically requires a fourth deposition step, or the use of external connections such as bond wires. The thickness of the conductor layers is also typically larger than the thickness of the core layers, therefore, the vertical distance over which connections must be made is larger in the pot core design. Furthermore, to form a closed magnetic core the upper and lower sections of the core have to be joined. The points where the two layers join is within the main flux path and can generate an unfavorable leakage flux leading to an increase in winding resistance, electromagnetic interference (EMI) and a reduction in component inductance.

2.3 Analytical design flowchart

Figure 5 displays the design flowchart for the development of a microinductor. The solenoid microinductor developed within this work formed a closed magnetic path. The accuracy of the analytical equations will be reduced with components that include air-gaps within the main flux path due to fringing effects. The equations within Fig. 5 are used for the theoretical data within Sect. 3.

3 Fabrication process

The solenoid component requires the manufacturing of three separate wafers. The fabrication of the upper and lower winding layers requires two different substrates, whilst the third wafer is dedicated to the process of the magnetic core of the component. A summarized fabrication process is given below:

Step 1 A 3 inch glass wafer is immersed in deionized water and cleaned for 3 h within an ultrasonic bath.
Step 2 A 100–200 nm thick titanium adhesion layer is deposited using electron beam evaporation. In order to decrease the resistivity of the seed conductive layer, the titanium layer is complemented by an additional 100–200 nm thick layer of nickel to allow for subsequent uniform electroplating across the surface of the wafer. A seed layer of Ti/Ni was used for all electroplated samples.
Step 3 A positive photoresist AZ 9260 is deposited to obtain the required conductor and core thickness.
Step 4 AZ 9260 is patterned with UV light and an acetate mask in a contact exposure mode. Energy dose of approximately 2,000 mJ for 90 μm thick resist is carried out and followed by 5 min of development immersed in a dilute 1:3 developer:deionised water.
Step 5 The upper and lower winding layers are DC electroplated at a thickness of 90 μm using either Cu or Ni. With the use of multiple AZ resist layers or a thick film resist such as SU-8 thicker winding layers could be have been fabricated (Brunet et al. 2002; Lorenz et al. 1997; Lorenz et al. 1998) at the expense of skin depth effects in the 0.5–1 MHz range.
Step 6 AZ is re-deposited and patterned, and gold bumps are electroplated. AZ is stripped with acetone. The seed

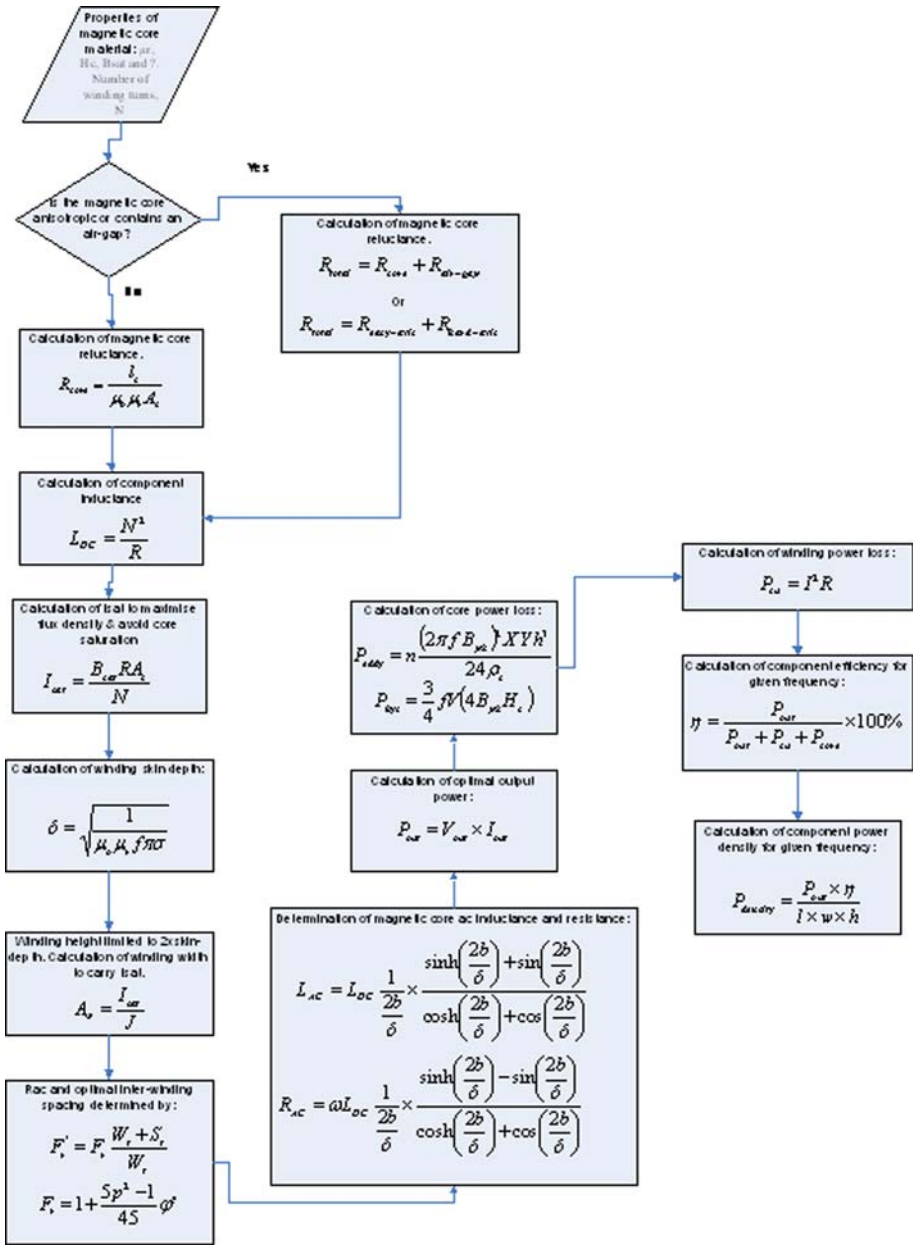

layer is etched and AZ insulation is deposited and patterned, Fig. 6 displays the component image and the 3D plot obtained by the white light phase shifting interferometer Zygo Viewmeter 5200.

Step 7 The magnetic core is electroplated and etched free. The upper and lower windings are diced.

Step 8 The lower insulation layer is coated with a 5 μm thick non-conductive adhesive layer. The tacky affect of the adhesive layer provides a degree of control when positioning the alloy. The core is placed on the adhesive layer and after 5 min is permanently fixed. The lower and upper winding layer is flip-chip bonded as shown in Fig. 7. The thermocompression bonding process required a temperature ramp from room temperature to 200°C, then 200–220°C followed by a cool down from 220°C to room temperature, and 40-60 g per bump of pressure. The Curie temperature of the alloys investigated ranged from 250–500°C (Daniel et al. 1999; Senseky 2005). Therefore, the bonding process did not have an adverse affect on the magnetic properties of the alloys.

Step 9 Titanium etchant, consisting of NaF 4 g, deionised water 100 ml and HCl 20 ml is used to release the glass substrate off the upper layer by etching the remainder of the upper seed layer, Fig. 8. The final component with 90 μm thick windings has dimensions 5 mm × 2 mm × 0.25 mm.

Fig. 5 The design flowchart of the microinductor

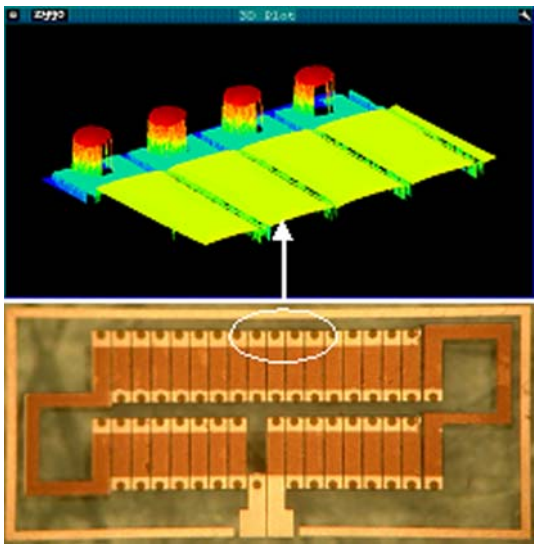

Fig. 6 Microinductor prior to core inclusion and flip chip bonding

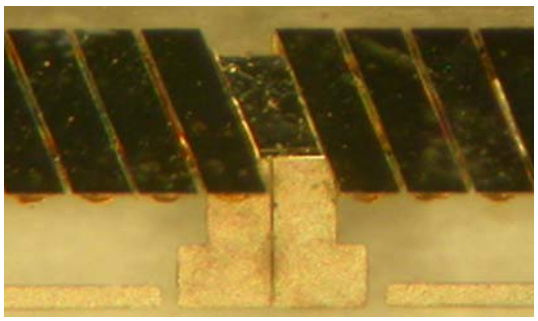

Fig. 7 Component after flip chip bonding. The view is through the upper glass substrate displaying the dark Ti seed layer

Fig. 8 Glass substrate removed from the upper layer, some residual Ti has remained on the winding. Some windings have been removed to expose the gold bumps underneath

Electrodeposition took place in the presence of a magnetic field in order to fabricate the anisotropic nickel-iron magnetic core. The permeability of the easy axis assumes a very large value at low frequencies if a small DC magnetic field is applied in the hard axis direction and equal to the anisotropy field of the magnetic film, Hk (300 A/m). Components fabricated and tested with the easy axis induced in the predominant length of the alloy exhibited increased inductance at lower frequency. The bandwidth of operation was reduced due to the inductance tail-off at reduced frequency as the permeability depends on the magnetization of the film. The magnetization is determined by two processes: domain wall motion and domain rotation. At low frequencies domain wall motion is the dominant mechanism. An applied field causes a shift of the domain walls. This motion results in a change of magnetization and flux density. Therefore, highly magnetized thin films will have larger permeability at low frequency. However, highly magnetized films (easy axis) will have very small restoring forces and therefore are unable to follow rapidly varying fields. At high frequencies, the domain rotation becomes dominant and is responsible for the permeability. It is hard for the large domains of the easy axis to rotate, while the small domains of the hard axis can rotate much more easily. Therefore only films with the hard axis which forms the majority of magnetic path length are considered.

An additional feature of magnetic field annealing is that hysteresis losses in nickel-iron films can, in principle, be eliminated if changes in magnetization proceed by coherent rotation of the magnetization in a single domain, instead of domain wall motion. A theoretical explanation of this process is based on the Stoner Wohlfarth Model (Cooper et al. 2005).

4 Component characterisation

The microinductor fabricated via flip-chip assembly is shown in Fig. 9. When the thin-film core is magnetically anisotropic, the respective hard and easy directions are indicated within Fig. 9.

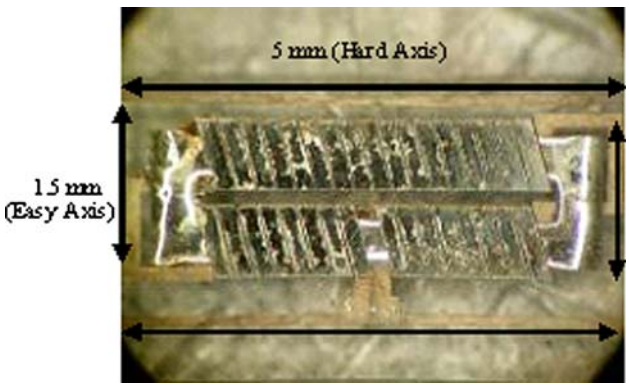

Fig. 9 Fabricated micro-inductor. The O-shape core is assembled between the windings layers prior to flip-chip bonding. The component is approximately 5 mm × 2 mm × 0.25 mm ($l \times b \times h$), respectively. When Ni-Fe is anisotropic the orientation of the Easy and Hard axes are indicated

A critical point in the performance of an inductor is the measurement of the inductance value as a function of frequency and the additional core losses. A Hewlett Packard 4192A LF-impedance analyzer was used to record the inductance, resistance and Q-factor over a frequency range of 1 kHz–10 MHz. The resistance value shown in Fig. 10 is for an air-core component. The reason for omitting the magnetic core was to remove core AC resistance from the recorded value. Therefore, the increase in resistance at high frequency from the R_{dc} value is due to skin and proximity affects with increasing frequency. The winding is 90 μm thick and at 1 MHz has a skin depth value of approximately 66 μm. Due to the winding consisting of a single layer and inter-winding spacing optimized, the proximity effect is minimized and the main contributor to the AC resistance is assumed to be the skin effect.

One important source of loss in a DC–DC converter is the DC winding resistance, R_{dc}, of the output inductor. This parameter defines the minimal loss condition of the inductor. For example, if $R_{dc} = 1$ mΩ, and the DC output current, $I = 100$ A, the inductor DC power loss is;

$$P = I^2 R_{dc} = 10\,(W) \tag{3}$$

If the converter were to provide 100 A at 0.75 Volts, the loss in efficiency due to the inductor R_{dc} would be 11.76%. This result demonstrates that the converter would be less than 89% efficient due to R_{dc} alone. Hence, it is important to have a winding configuration that minimizes R_{dc} whilst still meeting applied current and inductance criteria. The resistance of the components with the magnetic core included are shown in Fig. 11. The minor variation between experimental and analytical values may be due to the limitations of the 2D model representing the intrinsically 3D nature of the leakage and eddy current flux.

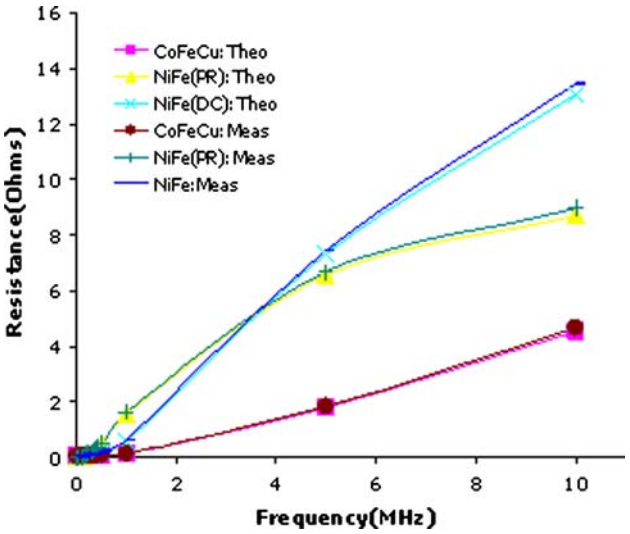

Fig. 11 Resistance of micro-inductor as a function of frequency. The resistance value includes the contributions of the windings and the core

Figure 12 displays the theoretical (theo) and measured values (meas) of the inductance with increasing frequency. Results between theory and experiment are in excellent agreement. The * sample indicates NiFe films that are magnetically anisotropic as indicated in Fig. 9.

The self resonant frequency (SRF) of an inductor is defined as the frequency at which the reactance becomes zero. The measured reactance increases linearly with frequency; hence the SRF induced by parasitic capacitance effects does not occur in the frequency range of interest.

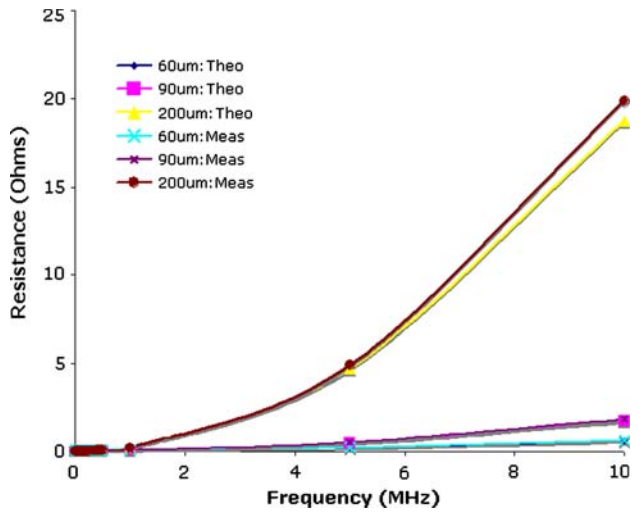

Fig. 10 Winding resistance vs. frequency for 90 μm thick copper windings

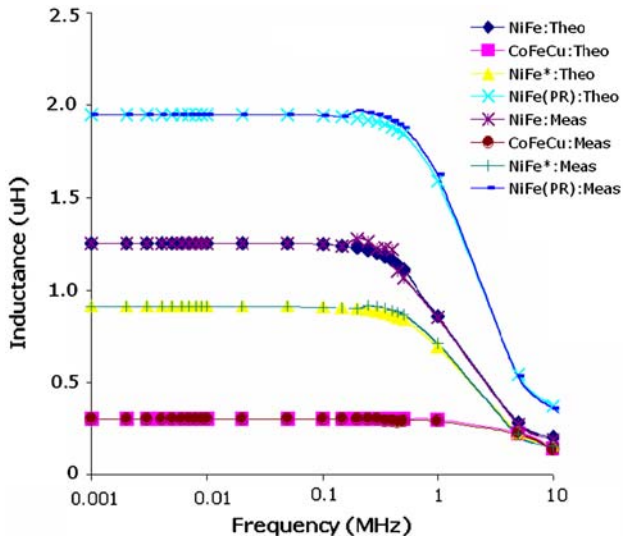

Fig. 12 Inductance of the electrodeposited alloys as a function of frequency

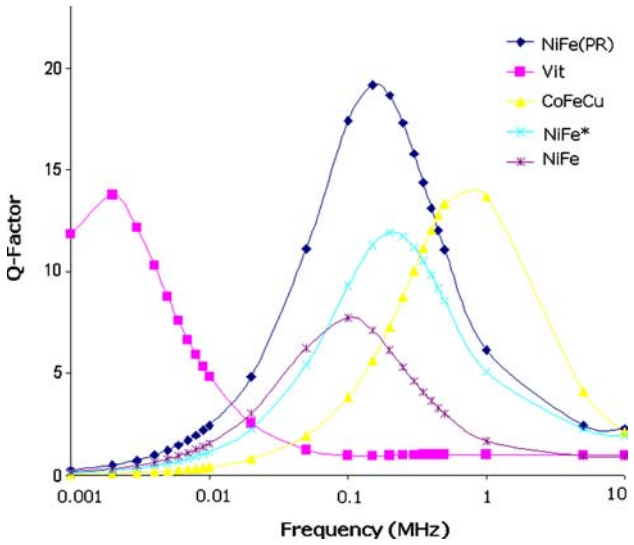

Fig. 13 Q-factor versus frequency for the electrodeposited alloys

The Q-factor of the electrodeposited alloys is displayed in Fig. 13. The maximum Q-factors of the alloys occurred in the 500 kHz–1 MHz frequency range indicating that the thin film dimensions are acceptable for operation within this range. Due to the properties of the CoFeCu core the 10 μm thick core layer remains below one skin depth at 1 MHz. The thicknesses of the components windings are less than twice the skin depth therefore AC winding losses are maintained at acceptable levels. Therefore the ratio of the stored power to dissipative power of the component, the Q-factor, was optimal in this frequency range.

The Q-factor response of the commercial alloy demonstrates the susceptibility of this particular film to skin depth effects. The skin depth effects increase the dissipative losses within the component, therefore reduce the Q-factor. The high Q-factor in the low frequency range is greatly reduced at 1 MHz for the CoFeCu film.

The maximum applied current can be determined by using the theoretical DC saturation current formula within Fig. 5. The performance of the prototypes is summarized in Table 1. K is taken to be equal to 4.44 for a sinusoidal waveform, and B_{sat} is used to maximize the power density of the component.

The saturation current of the Vitrovac material is only 1.33 mA. Hence, high efficiency is achieved at the expense of power density. An appropriate reduction in the number of windings and increase in core area via lamination will result in the same overall inductance. This would reduce the major Joule loss mechanism, winding loss, and allow windings of larger dimensions to be fabricated in order to apply greater current. The 90 μm thick windings limit the maximum current to 180 mA which is well beneath the saturation current of the CoFeCu components. An optimal component design process is therefore required.

Table 1 Microinductor performance for different core materials at 0.5 mhz

Parameter	NiFe	NiFe*	Vit	NiFe (PR)	CoFeCu
Isat (mA)	100	137	1.32	66	180
L (μH)	1.07	0.86	15.5	1.87	0.28
Vin (V)	0.29	0.29	0.36	0.28	0.51
Pout (mW)	29	40	0.47	18.48	91.8
Peddy (mW)	7.23	7.23	3.47	2.86	24.6
Phys (mW)	0.198	0.03	0.02	0.08	0.11
Pcu (mW)	0.5	0.9	0.00008	0.21	1.62
Efficiency (%)	78	82	X	85	77
Power Density (W/cm^3)	7.8	11.3	X	5.46	24.7

5 Optimal design process

A simplified design procedure for optimum solenoid component is outlined within this section. The optimization is performed in two instances in reference to the CoFeCu prototype in section III: (1) the aim of the first design is to maintain the inductance value whilst increasing the power density significantly and improve efficiency, and (2) the primary aims of the second design are two maintain inductance and improve efficiency. The CoFeCu alloy is chosen as the material for optimization because of its good relative permeability, small coercivity, reasonable resistivity and its largest saturation current (1.24 A). Once a frequency is selected, in this case 0.5 MHz, skin depth values for the windings and core laminates are 93 μm and 17.4 μm, respectively. The inductance required for the prototype will be 0.3 μH (Fig. 12). The core area and numbers of turns are therefore:

$$LI = NA_c B \tag{4}$$

and the area of the component is:

$$A_c = \frac{LI}{BN} \tag{5}$$

Design constraints are included at this stage. Each CoFeCu laminate will have a thickness of half the skin depth and the number of laminations will be restricted to 10. The number of laminations affects component manufacturability and cost such that N is only 11 turns in our case. The maximum applied current is 1.24 A, PCB current density is 10 A/mm^2 and winding height is restricted to twice the skin depth. The dimensions and performance of the optimized component can therefore be calculated and are given in Table 2.

The optimized component (1) produces a 6% increase in efficiency and a sevenfold increase in power density. Conventional inductors and transformers will normally operate with efficiency in the range of 90–95%. Hence, the

Table 2 Optimised performance and parameters

Dimensions	Optimized component (1)	Optimized component (2)	Prototype Component
Number of turns	11	33	33
Turn thickness	180 μm	90 μm	90 μm
Turn width	550 μm	200 μm	200 μm
Turn spacing	55 μm	20 μm	20 μm
Laminations	2	10	1
Lamination thickness	5 μm	1 μm	10 μm
Lamination width	500 μm	500 μm	500 μm
Lamination insulation	5 μm	5 μm	5 μm
Performance	Optimized component	Prototype component	Prototype component
V_{in}	0.17	0.51	0.51
P_{out}	0.2108 (W)	0.0918 (W)	0.0918 (W)
B_{pk}	1.4 (T)	1.4 (T)	1.4 (T)
P_{eddy}	5.54 (mW)	0.22 (mW)	24.6 (mW)
P_{hys}	0.57 (mW)	0.11 (mW)	0.11 (mW)
P_{Cu}	184 (mW)	1.62 (mW)	1.62 (mW)
Efficiency (%)	83	97	77
Power density (W/cm^3)	174.8	30.83	24.7

application would have to greatly benefit from the increase in power density to tolerate the moderate level of efficiency. Optimized component (2) uses the data from the prototype to identify eddy current core loss as the main loss mechanism. The core is reduced to ten 1 μm laminates and via this adjustment improves efficiency by 20%. Comparing the two optimized components, a trade-off between output power efficiency and power density is evident.

6 Conclusions

Micromachined inductors with different magnetic cores have been fabricated on glass using micromachined techniques borrowed from the LIGA process. From the results, windings parasitic capacitances do not appear to significantly affect inductor performance over the measured frequency range. Eddy currents and parasitic capacitance become significant at higher frequency. The analytical results using the two dimensional model agree well with the experimental values measured for the inductance and resistance. The minor increase in resistance is attributed to the hysteresis resistance that is omitted from the model and parasitic resistance induced by leakage flux.

The solenoid winding is normally a 3D structure that is difficult to fabricate with micro-machining techniques. This type of device can be susceptible of high resistance interconnects. The novel assembly process of the windings using thick film electroplating and flip-chip bonding, overcomes these issues. The results within Fig. 10 indicate that the solenoid winding has a low winding resistance, which is essential to efficient component operation. The results shown in Fig. 12 demonstrate that the DC inductance equation within the design flowchart is only valid for uniform flux density. As a rule of thumb for laminated core, a laminate sheet should not have a thickness greater the skin depth for a given frequency.

The performance of the commercial alloys is hindered by the thickness and high relative permeability of the film as shown in Fig. 13. Electrodeposited alloys are better suited to the application due to the ability to vary the film thickness and relative permeability via magnetic field annealing or deposition current waveform. These processes avoid the need for additives that may greatly reduce saturation flux density, which is a purely compositional dependent value. Pulse reverse plating achieved a higher inductance than with other electrodeposition techniques and the anisotropic permalloy had a greater bandwidth of operation than the "traditional" DC permalloy.

The challenge of developing inductors and transformers for MHz DC–DC converter operation requires the development of suitable core materials and manufacturability of laminated layers. This fact is demonstrated by the results within Tables 1 and 2. The micro-inductor presented in this article has proved that an efficient component can be manufactured via an inexpensive UV LIGA and electroplating process.

Acknowledgments Thanks are extended to Prof Cywinski for the VSM data performed at the University of Leeds, and to Raytheon Systems Limited for performing the resistivity measurements. This work was made possible through the funding of the Scottish Consortium in Integrated Micro Photonic Systems (SCIMPS) funded by the Scottish Funding Council under the Strategic Research Development Grant scheme.

References

Brunet M et al (2002) Thick photoresist development for the fabrication of high aspect ratio magnetic coils. IoP J Microeng Micromech 12:444–449

Cooper EI et al (2005) Recent developments in high-moment electroplated materials for recording heads. IBM J Res Dev 49(1):103–126

Daniel L et al (1999) Design of microfabricated inductors. IEEE Trans Power Electron 14(4):709–723. doi:10.1109/63.774209

Flynn D et al (2007) Study of a solenoid microinductor operating in the MHz frequency range. IoP J Microeng Micromech 16:1811–1818

Goldberg AF (1988) Development of magnetic components for 1–10 MHz DC–DC converters. PhD thesis, Massachusetts Institute of Technology

Huljak RJ et al (2000) Where are power supplies headed? APEC fifteenth annual conference IEEE, vol 1, pp 10–17. doi:10.1109/APEC.2000.826076

International Technology Roadmap for Semiconductors (2001) Edition System Drivers (ITRS)

Jagielinski T (1990) Materials for future high performance magnetic recording heads. MRS Bull 15(3):36–44

Kohmoto O (1991) Recent developments of thin film materials for magnetic heads. IEEE Trans Magn 27(4):3640–3647

Lorenz H et al (1997) SU-8 a low cost negative resist for MEMS. J Micromech Microeng 7:121–124. doi:10.1088/0960-1317/7/3/010

Lorenz H et al (1998) High-aspect ratio, ultrathick, negative-tone near-UV photoresist and its applications for MEMS. Sens Actuators A 64:33−39

Lotfi AW et al (2001) Issues and advances in high-frequency magnetics for switching power supplies. Proc IEEE 89(6):833–845

Power Technology Roadmap PSMA (2000). www.psma.com. [Online]

Wong FK (2004) High frequency transformer for switching mode power supplies. PhD thesis, Griffith University, Brisbane, Australia

Senseky MK (2005) Electromagnetic generators for portable power applications. PhD Thesis, University of California, Berkeley

Sullivan CR et al (2003) Measured electrical performance of V-groove inductors for microprocessor power delivery. IEEE Trans Magn 39(5):3190–3192